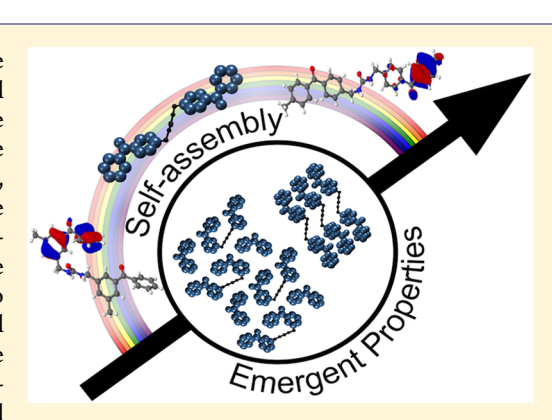


Enhancing the Stability of Photogenerated Benzophenone Triplet Radical Pairs through Supramolecular Assembly

Baillie A. DeHaven,[†] Dustin W. Goodlett,[†] Ammon J. Sindt,[†] Niklas Noll,[†] Martina De Vetta,^{‡,§} Mark D. Smith, Corey R. Martin, Leticia González, and Linda S. Shimizu*,

Supporting Information

ABSTRACT: Supramolecular assembly of urea-tethered benzophenone molecules results in the formation of remarkably persistent triplet radical pairs upon UV irradiation at room temperature, whereas no radicals were observed in solution. The factors that lead to emergent organic radicals are correlated with the microenvironment around the benzophenone carbonyl, types of proximal hydrogens, and the rigid supramolecular network. The absorption spectra of the linear analogues were rationalized using timedependent density functional theory calculations on the crystal structure and in dimethyl sulfoxide, employing an implicit solvation model to describe structural and electronic solvent effects. Inspection of the natural transition orbitals for the more important excitation bands of the absorption spectra indicates that crystallization of the benzophenonecontaining molecules should present a stark contrast in photophysical



properties versus that in solution, which was indeed reflected by their quantum efficiencies upon solid-state assembly. Persistent organic radicals have prospective applications ranging from organic light-emitting diode technology to NMR polarizing agents.

INTRODUCTION

The supramolecular assembly of small molecules through noncovalent interactions is proving to be a convenient approach in the design of hierarchical materials. $^{1-3}$ Controlled organization of discrete functional groups can enhance chemical and physical properties. For example, the solid-state assembly of perylene bisimide dyes form transistors with ntype charge transport properties^{4,5} and π -conjugated materials that exhibit enhanced luminescence. 6,7 Thus, further insight into how structure influences physical function is of great importance for the design of synergistic materials with properties tailored to specific applications. Here, we compare the impact solid-state assembly has on the photophysics of three benzophenone (BP)-containing molecules. We report that organization of BP units within distinct solid-state environments quenches the lifetime and modulates the quantum yield of phosphorescence. Moreover, remarkably persistent radicals are generated upon UV irradiation at room temperature. The quantity and stability of these radicals vary with the chemical environment that surrounds the key carbonyl unit (Figure 1). Thus, control over solid-state assembly of BP molecules can alter photophysical properties and lead to the generation of persistent radical pairs with potential applications ranging from organic light-emitting diode (OLED) technology to NMR polarizing agents.^{8–10}

Benzophenone, a prominent photosensitizer, was first reported to generate organic ketyl radicals in 1891. 11 Inherent high reactivity makes electron paramagnetic resonance (EPR)

characterizations difficult as they are known to dimerize in solution, forming benzopinacol. 12 Radicals generated by BP in solution are unstable and are typically only observed using EPR at low temperatures or through one-electron reduction to form the radical anion. 13,14 Previously, we reported a bis-urea macrocycle (1) that contains two BP units, which assembles into hexagonally packed columnar structures via robust urea hydrogen-bonding interactions. 15 Preorganization of the sensitizer impacted its photophysical properties by dramatically decreasing the quantum yield and lifetime. 16 Most intriguingly, UV irradiation of this crystalline solid gave rise to organic radicals that persisted for weeks at room temperature when stored in the dark. 10 High-field and variable-temperature Xband EPR studies accompanied by simulations suggested that UV irradiation of the crystals results in a resonance-stabilized radical pair through hydrogen abstraction. 10 Our hypothesis is that BP in the excited state abstracts a hydrogen atom from a nearby molecule to form ketyl-containing radical pairs.

Herein, we examine the chemical and photophysical properties of self-organized structures of BP-containing linear analogues and macrocycles (Figure 1A). Macrocycles 1 and 4 vary the position of BP within the cyclic framework to probe how orientation of the chromophore influences its crystalline packing. Linear analogues 2 and 3 comprise two BP molecules covalently tethered through a single methylene urea group and

Received: August 8, 2018 Published: September 13, 2018

13064

[†]Department of Chemistry and Biochemistry, University of South Carolina, Columbia, South Carolina 29208, United States *Institute of Theoretical Chemistry, Faculty of Chemistry, University of Vienna, Währinger Strasse 17, 1090 Vienna, Austria

Journal of the American Chemical Society

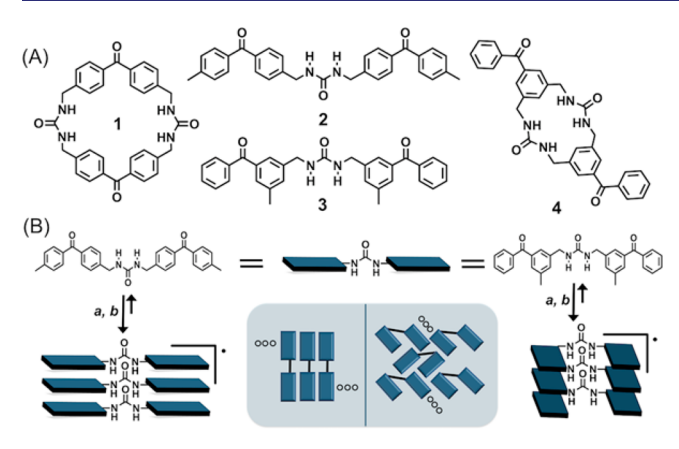


Figure 1. Self-assembly modulates the photophysics of BP derivatives and gives rise to emergent organic radicals. (A) Structures of ureabased BP-containing macrocycles and linear analogues, 1–4. (B) Monomers 2 and 3, presented as planar for simplicity, assemble through hydrogen-bonding interactions. UV irradiation gives rise to persistent radicals as an emergent property. Reagents and conditions: (a) crystallization; (b) UV irradiation (360 nm, rt, under N_2). Inset: Top-down assembly motif of the BP sensitizer in each crystal structure, 2 (left) and 3 (right).

assemble through urea hydrogen-bonding interactions. The positions of the methyl substituents, *meta* or *para* with respect to the BP carbonyl, were varied across two different structures in order to explore their influence on crystal packing as well as determine the types of H-abstraction sites near the carbonyl oxygen. Our goals are to examine how orientation of the BP sensitizer, as well as its relative position with respect to H-abstraction sites, impacts subsequent photophysical properties and to determine if these assembled BP linear analogues also display the ability to form persistent radicals upon UV irradiation or if this emergent property is a function of the assembled macrocycles.

■ RESULTS AND DISCUSSION

The macrocycles and linear counterparts were synthesized in three to four steps using a simple alkylation of a protected urea (triazinanone) as the key step. The protected analogue of 2 and macrocycle 4 were structurally characterized (see the Supporting Information). Colorless solvent-free crystals of 2 and 3 were obtained by recrystallization. Unfortunately, attempts to crystallize 4 through slow cooling, vapor diffusion, and microcrystallization techniques did not yield single crystals. We are currently screening a wide range of crystallization techniques, including conditions with potential co-crystal formers.

Crystals of **2** were obtained as transparent plates through slow cooling in a hot acetic acid solution (120 °C, 6 mg/mL). The sample crystallized in the triclinic system in the acentric space group P1 (no. 1). The conformation of **2** is linear, with the two BP units outstretched on both sides of the urea tether (Figure 2A). The two BP carbonyl groups of the monomer are aligned antiparallel, likely to minimize the dipole moment. Bifurcated urea hydrogen-bond interactions guide the assembly of **2** with N–H···O distances ranging from 2.873(2) to 2.968(2) Å (Figure 2B,C). The BP sensitizer is ordered down the *ab* crystallographic plane, resulting in a lamellar packing motif with aryl groups organized in an edge-to-face pattern and $C_g \cdot \cdot \cdot C_g$ distances (C_g = ring centroid) ranging from 4.601(2) to 4.825(2) Å. The C–H···C $_g$ distances vary from 3.419(4) to

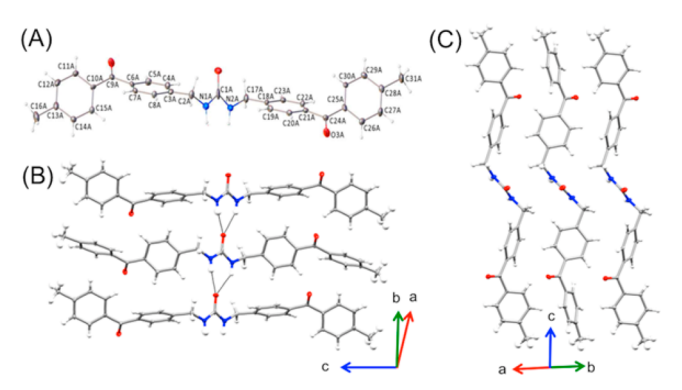


Figure 2. Single-crystal X-ray diffraction (SC-XRD) of linear analogue **2**, which crystallizes through slow cooling in acetic acid in the triclinic system as transparent platelets. (A) Thermal ellipsoid plot. (B) View of the urea hydrogen-bond interactions that stack BP units on top of each other and orient the aryl rings in an edge-to-face motif down the urea tape. (C) Top-down view of the urea groups showing that the edge-to-face aryl packing pattern is maintained between neighboring BP units in two directions.

3.637(3) Å, with angles ranging from 127 to 135°. The BP carbonyl oxygens reside in close proximity to aryl protons on closely packed molecules of 2 with C=O···H distances as close as 2.60 Å.

Slow evaporation of 3 in dichloromethane (1 mg/1.6 mL) resulted in the formation of transparent needle-like crystals in the monoclinic system in the acentric $P2_1$ space group. The profile of 3 is distinct, conforming to a C shape with both BP components oriented in close proximity and $C_g\cdots C_g$ distances of 8.94 Å between alkyl-substituted aryl groups. The two BP carbonyls of 3 are oriented in the same direction, although the carbonyls on neighboring molecules are opposing in direction. Predictable bifurcated urea—urea hydrogen-bonding interactions stack the sensitizer down the a-axis with N–H···O distances ranging from 2.800(6) to 2.809(6) Å (Figure 3A). This assembly orients the BP units in a herringbone pattern

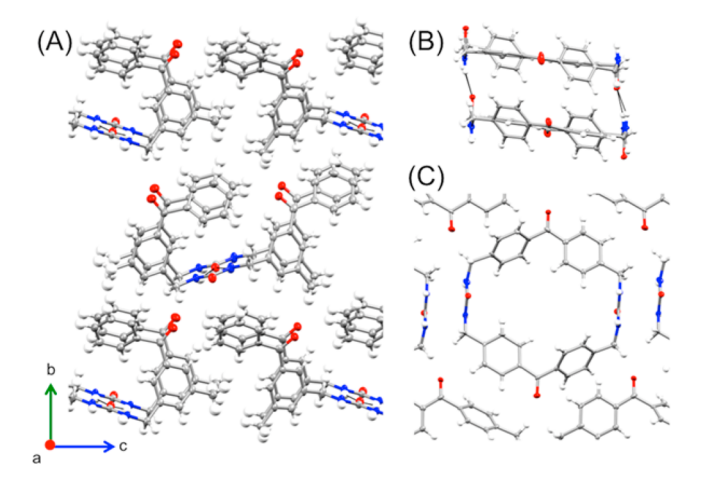


Figure 3. SC-XRD analysis of analogue 3 and macrocycle 1. (A) Slow evaporation of 3 forms transparent needle-like crystals in the monoclinic system, with BP units assembled in a herringbone pattern along the b-axis. The aryl rings are parallel displaced down the a-axis. (B) Macrocycle 1 crystallizes in the monoclinic system as needle-like crystals, with BP units stacked down the a-axis, resulting in edge-to-face aryl packing down the column. (C) Columns pack hexagonally staggering BP units across the c-axis.

Table 1. Measured Photophysical Properties of BP and the BP-Urea Molecules in DMSO Solution Compared to Those in the Solid-State

photophysical properties		1	2	3	4	BP
$\varepsilon \left(\mathrm{M^{-1} cm^{-1}} \right)$		622 ^a	449	317	297	342 ^a
λ_{\max} abs (nm)	solution	$\pi\pi^*$, 270°	$\pi\pi^*$, 260	$\pi\pi^*$, 256	$\pi\pi^*$, 265	$\pi\pi^*$, 270°
		$n\pi^*$, 345 ^a	nπ*, 335	nπ*, 340	nπ*, 340	nπ*, 345°
	crystals	$\pi\pi^*$, 355 ^a	$\pi\pi^*$, 382	$\pi\pi^*$, 374		$\pi\pi^*$, 381
λ_{max} em (nm)	solution	435 ^a	474	465	502	435 ^a
	crystals	489 ^a	528	526		450 ^a
τ (ns)	solution		1.5	2.0	1.5	
	crystals	0.32 ^a	0.94	1.3		23000 ^a
φ (%)	solution		<0.3	<0.3	<0.3	
	crystals	<0.1 ^a	5.0	< 0.3		0.5 ^a

^aValues obtained from ref 16.

along the *b*-axis, whereas the aryl rings are parallel displaced down the *a*-axis with a distance of 4.511(3) Å from centroid to centroid. The carbonyl oxygens reside in close proximity to benzyl and aryl protons on proximal molecules of 3 with C= O···H distances of 2.60 Å to methyl hydrogens, 2.88 Å to methylene protons, and 2.64 Å to aryl hydrogens.

In comparison, previously reported 1 crystallizes as transparent needle-like crystals in the monoclinic system in the $P2_1$ space group by slow cooling a hot dimethyl sulfoxide (DMSO) solution from 120 °C. ¹⁵ The two BP carbonyl carbons of the monomer are 10.2 Å apart and orient the carbonyl oxygens pointing outward toward the exterior of the macrocycle. Ureaurea hydrogen-bond interactions drive assembly, stacking the BP molecules down the a-axis and aligning the aryl rings in an edge-to-face motif, with C–H···Cg distances ranging from 3.559(6) to 3.597(7) Å and angles from 124 to 130° (Figure 3B). The columns encapsulate disordered DMSO molecules. The macrocycles are hexagonally packed, and the BP units are staggered like brickwork along the c-axis. ¹⁵ The BP carbonyl oxygens are in close proximity to neighboring methylene and aryl hydrogens, with C=O···H distances of 2.41 and 2.68 Å, respectively (Figure 3C).

To probe how crystal packing of BP units impacts the overall photophysics, we measured the absorption, emission, lifetime, and quantum yield for each sample in the solid-state and in argon-purged solutions of DMSO. 16 DMSO, an aggressive solvent, was selected because macrocycles 1 and 4 are poorly soluble. Absorption and emission spectra are strongly influenced by solvent polarity, so samples were kept consistent when possible. Table 1 compares these measurements with unsubstituted BP and 1. For both linear analogues and macrocycles, the absorption spectra in solution maintained the major spectroscopic properties of BP, with a strong $\pi\pi^*$ band ranging from 256 to 270 nm and a weak spin-forbidden $n\pi^*$ transition from 335 to 345 nm. The molar absorptivity for these compounds ranges from 297 to 622 M⁻¹ cm⁻¹, with the para-substituted compounds exhibiting values higher than those of unsubstituted BP and the meta-substituted values being lower (Figures S24-S26). In comparison, solid-state assembly of 1-3 induces an overall bathochromic shift in the spectrum, $\lambda_{\text{max}} = 355-382$ nm, with broadening in the UV/vis region. This red shift is similar to what is observed upon formation of J-aggregates with dyes, 17 although this is not a perfect analogy as the BP chromophore is not planar.

The absorption properties of 2 and 3 were examined through time-dependent density functional theory (TD-DFT) calculations to characterize the excited states of these

molecules. This was done by calculating the absorption spectra of 2 and 3 using the crystal structures in the gas phase and an optimized geometry with the polarized continuum model (PCM)¹⁸ in DMSO. The excited states were calculated at the ω B97XD¹⁹/6-31+G**²⁰ level of theory. More computational details are given in the Supporting Information. During optimization of 2, the average dihedral angle between the two rings of the BP unit shifted from 26.9 to 31.3° (Figure \$35). Additionally, the benzenes directly connected to the urea spacers move from being in plane with each other and roughly perpendicular to the urea unit to a more contorted structure. Nevertheless, the spectrum calculated with implicit solvation in DMSO shows good agreement with the experiment, being only slightly blue-shifted (5 nm) with respect to the main absorption peak raised by $\pi\pi^*$ transitions. The computations also find the dark $n\pi^*$ transition as the lowest excited state. In comparison, the spectrum of 2 calculated for the crystal structure in the gas phase is shifted by 119 nm to higher energies with respect to the experimental solid-state spectrum (Figure 4A). Even though the excitation energies differ, the

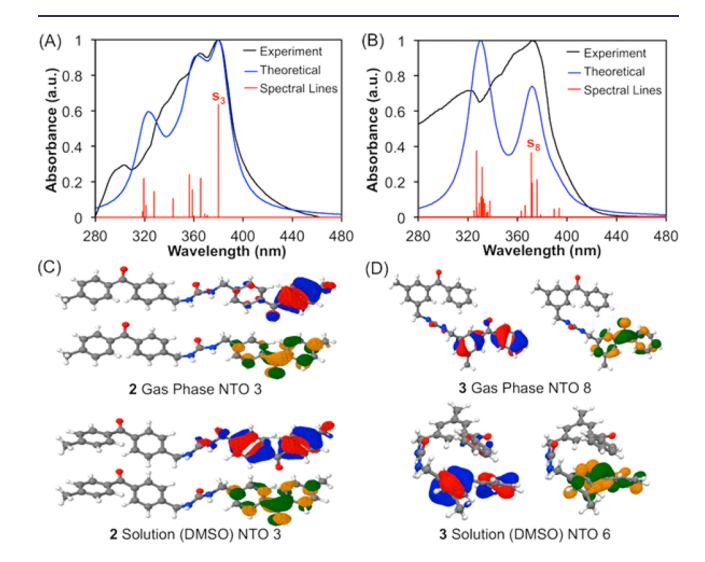


Figure 4. Excited states of 2 and 3 were characterized using TD-DFT calculations. The normalized experimental solid-state absorption spectra of (A) 2 and (B) 3 are compared to their calculated spectra in the gas phase, including the corresponding spectral lines; the numbers indicate the electronic excited state. Natural transition orbitals for the main transitions of (C) 2 and (D) 3 in the gas phase compared to those in solution, where red/blue = occupied orbital and yellow/green = virtual orbital.

shape of the experimental spectra is reproducible and allows for the assignment of the lower energy absorption peaks to their corresponding electronic excitations. Similarly, the computed absorption spectra for 3 using the crystal structure geometry in the gas phase gave roughly the same shape with two intense absorption bands raised by the $\pi\pi^*$ transitions (Figure 4B). Similar to 2, this spectrum was blue-shifted by 135 nm compared to the experiment. As seen before, the $n\pi^*$ transition was found as the lowest excited state. The calculated spectrum for the structure optimized in solution was again only slightly shifted in comparison to that in the experiment (4 nm).

As seen in Figure 4C,D, there is a stark contrast between the occupied natural transition orbitals (NTOs) for 2 and 3. In solution, the occupied NTO of 2 covers the entire BP unit including both benzene rings, whereas the corresponding occupied NTO in the gas phase with the crystal structure geometry shows contributions from only one of the BP benzene rings. Moreover, many of the NTOs contributing to the finer structure for the gas-phase spectrum show the electron density localized on only one of the two aromatic rings of the BP units (Figure S31). In comparison, 3 shows little difference in the electron density distribution moving from the gas phase to solution. In both cases for 3, the occupied NTO covers the entire BP unit. These calculations suggest that 2 should present a stark contrast in its photophysical properties when in the solid-state versus in solution, although we do not expect strong media effects for 3.

The emission spectra recorded in solution (DMSO, 0.9-1.0 mM) exhibited transitions ranging from 435 to 502 nm and displayed an overall red shift upon solid-state assembly, $\lambda_{\rm em}$ = 450-528 nm. The phosphorescence lifetimes of 2 and 4 in solution (DMSO, 0.9 mM) were the shortest at 1.5 ns, whereas 3 exhibited a slightly longer lifetime at 2.0 ns. Upon solid-state assembly, the lifetimes of 2 and 3 were slightly quenched to 0.94 and 1.3 ns, respectively. Such deactivation in lifetime suggests that these compounds are prone to intermolecular self-quenching similar to other BP compounds. 21,22 A comprehensive study on this phenomenon by the Garcia-Garibay group demonstrated that the lifetimes of BP nanocrystals with electron-donating substituents are dramatically shorter than those in solution, varying over 9 orders of magnitude depending on the electron-donating ability of the substituents.²² This is attributed to intermolecular selfquenching via a charge transfer mechanism.²² The shorter observed lifetimes for 2 and 3 in the crystals are consistent with these previous reports, as the alkyl groups are mildly

The phosphorescent quantum yields of 2-4 in DMSO solution (25 µM and 1 mM) displayed efficiencies of less than 0.3% in all cases. The low quantum efficiency is attributed to unrestricted rotations and vibrations of the sensitizer when allowed to move freely in solution. Interestingly, crystallization of 2 dramatically increased its quantum yield to 5.0% but did not influence 3 as predicted by computation. The calculations suggest that the solid-state geometry of 2 forces each of BP's benzene rings to act independently, whereas in solution, the linear analogue is able to orient itself so that both benzenes participate in the excitation of the π bands, resulting in a loss of independent chromophores. This demonstrates that the higher quantum yield observed for 2 upon solid-state assembly is likely due to suppressed mobility when locked within the crystalline lattice. Literature reports also correlate suppressed mobility with increased quantum yields. 23-25 Recent studies

have shown that halo-substituted BP units exhibit enhanced phosphorescence when organized in the solid-state.²³ In solution, the quantum yields were sufficiently diminished, but they became highly emissive when frozen with liquid nitrogen.²³ Here, we show that restricting molecular motion of BP enriched a radiative decay pathway of the triplet excited state when only one of BP's benzene rings participates in the excitation process.

Typically, upon Franck–Condon excitation, BP undergoes rapid intersystem crossing (ISC) from $S_1 \rightarrow T_2 \rightarrow T_1$ excited states, 26 which can abstract nearby hydrogens to form ketylcontaining radical pairs as well as undergo other excited state or thermal processes. 27 Scheffer proposed that intramolecular photochemical H-abstraction is preferred when the C=O···H distance is below the sum of the van der Waals radii of the oxygen and hydrogen atoms (2.72 Å), 28 whereas others have observed intermolecular H-abstraction by BP with C=O···H distances as far as 3.13 Å. 29,30 Figure 5 compares the

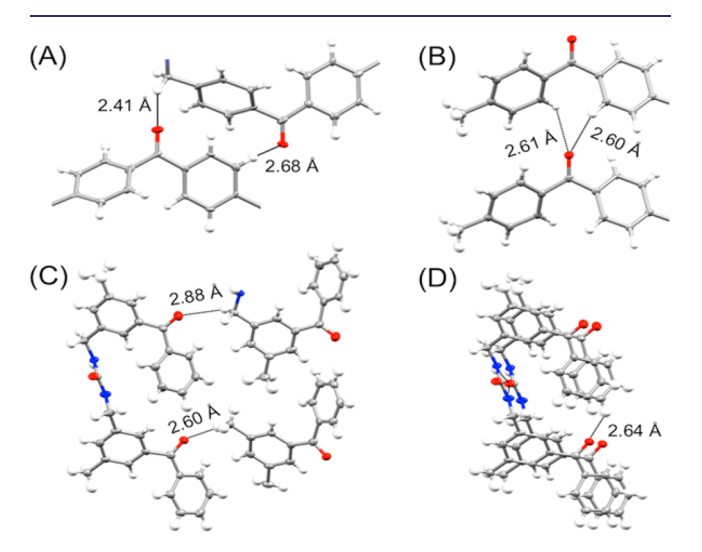


Figure 5. Comparison of the microenvironments around the BP carbonyl obtained from the SC-XRD of compounds 1-3. (A) 1 has neighboring aryl and benzyl CH_2 protons. (B) Carbonyl of 2 resides in close proximity to only neighboring aryl protons. (C) More complex structure of 3 is oriented close in space to two types of benzyls protons (CH $_3$ and CH $_2$) as well as (D) aryl protons.

microenvironment around the BP groups in the three systems and shows that there are, indeed, closely preorganized hydrogens (<2.72 Å to BP oxygen). The BP carbonyl in 1 is organized more closely to neighboring benzyl protons (2.41 Å) versus the harder to abstract aryl protons (2.68 Å). In comparison, in 2, the carbonyl oxygen is in close proximity to only the aryl protons (2.60 Å), which have a higher bond dissociation energy (BDE). BP has been found to abstract hydrogen atoms from benzene rings, albeit slowly.³¹ Our hypothesis is that UV irradiation of 2 crystals may produce a triplet radical pair in an efficiency lower than that for 1. Finally, for 3, there are proximal benzylic CH₃ (2.60 Å), benzylic methylenes (2.88 Å), and aryl protons (2.64 Å), which suggests that several different triplet radical pairs could be formed. Simple BDE arguments predict the ketyl radicals may be formed more easily in compounds 1 and 3 as compared with 2, which only contains close aryl hydrogens, as homolytic BDEs are lower for benzyl protons versus aryl (88 kcal/mol vs

111 kcal/mol, respectively). 32 Despite this, BP has been known to abstract all three types of protons.^{29–3}

In an effort to correlate structure with the formation and stability of the UV-generated triplet radical pairs, we turned to X-band EPR spectroscopy. First, EPR spectra were recorded on solutions of 2 and 3 in dichloromethane (1 mM) pre- and post-UV irradiation (1 h). (EPR experiments were performed in N2 degassed dichloromethane; DMSO was not selected as the water impurity absorbed the microwaves.) As expected, no EPR signal was observed pre- or post-UV, indicating that any ketyl radical formed is quickly terminated in solution (Figure S38). Upon UV irradiation, the linear analogue solutions vellowed and showed only minor spectroscopic changes by absorption spectroscopy (Figure S43).

Next, solid-state EPR spectra were recorded on triply recrystallized samples of 2 and 3 (\sim 10 mg) pre- and post-UV. (The samples were triply recrystallized to ensure that any radical generated is a result of BP photochemistry.) After 1 h of UV irradiation, the transparent crystals of 2 turned reddishbrown in color (Figure 6A), whereas the needle-like crystals of

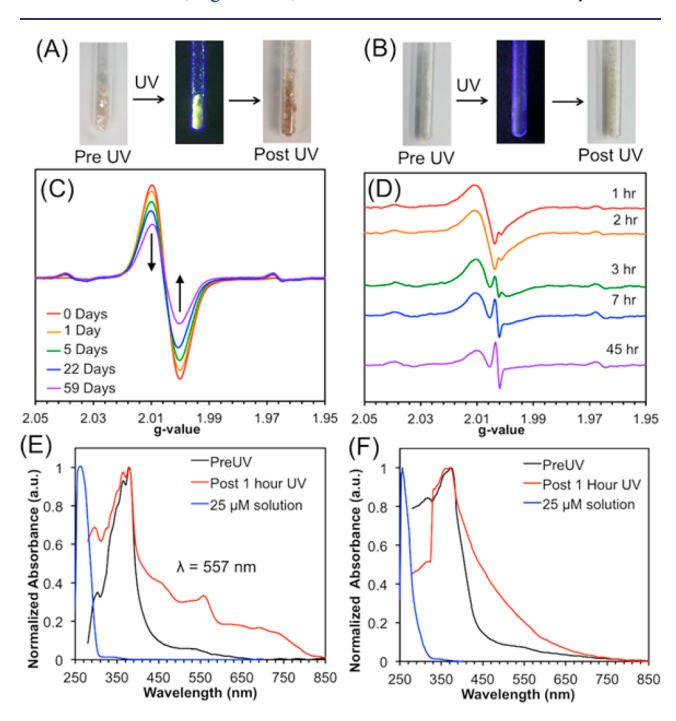


Figure 6. Photophysical properties of the triply recrystallized samples of 2 and 3 pre- and post-UV irradiation. (A) Transparent crystals of 2 exhibit green fluorescence under UV light and become brown-red upon UV irradiation. (B) Needle-like crystals of 3 show quenched emission and only slightly yellow in color after UV irradiation. (C) EPR of 2 post-UV and subsequent dark decay study demonstrating that the radicals are persistent for several days at rt. (D) EPR of 3 exhibits persistent radicals after irradiation with a significant change in EPR line shape within 2 h post-UV. Comparison of absorption spectra of (E) 2 and (F) 3 in solution and their recrystallized solids pre- and post-UV irradiation for 1 h; the new absorbance band in 2 at $\lambda = 557$ nm is labeled.

3 became opaque upon removal from the mother liquor and showed a slight yellowing in color upon UV irradiation (Figure 6B). UV irradiation of the crystals resulted in the formation of radicals in both 2 and 3 with g values of 2.005 and 2.007, respectively (Figures 6 and S39). Irradiation of 2 crystals gave rise to an isotropic EPR signal. The EPR line width of 3 was

similar, but a weak second transition was observed at g = 2.003. A g value of 2.003 has previously been attributed to the BP ketyl.33

The concentration of radical pairs generated after 1 h of UV irradiation was approximated using a calibration of standard solutions of TEMPO in benzene (Figure S40). 10,34 Double integration of the EPR signals provides the overall area of the spectra, which were then compared to the TEMPO calibration. One hour UV irradiation of 2 generated the same amount of radical as a 0.053 mM solution of TEMPO in benzene, suggesting that approximately 1 in 5000 molecules of 2 has a radical. In comparison, after similar UV irradiation, host 1 showed ~1 in 30000 molecules has a radical, 10 whereas the linear analogue 3 shows radicals in ~1 in 25000 molecules (similar to a 0.009 mM TEMPO solution). The amount of UV-generated radical formed increases with longer irradiation times. This result shows that 2 generates approximately 5 times more radical than 3 after 1 h of UV irradiation and demonstrates that radical formation is not deterred by higher homolytic BDEs. However, it is possible that the persistence of the radical pair is playing a role in the observed concentration difference.

Therefore, the persistence of the radicals was probed using dark decay studies where the samples were stored at room temperature in the dark after irradiation, and EPR spectra were recorded over time. The dark decay study of 2 shows that there was little change in line shape and g value (2.005) 140 days post-UV irradiation (Figure 6C). Sixty days after UV irradiation, the area of the EPR signal retained half its initial amount, demonstrating the remarkable persistence of the radicals of 2 (Figure S41). In comparison, dark decay studies on recrystallized 3 showed a faster decay and exhibited dramatic changes in the EPR line shape (Figure 6D). Post-UV, the broad EPR line exhibited a g value of 2.007 with a weak transition at g = 2.003. Two hours after irradiation, the EPR signal retained a similar line shape, although a stark change was observed between 2 and 3 h after irradiation, with an increase in population of radicals at g = 2.003. The overall line width of the spectra remained similar, but the area of the signal was decreased by half just 45 h after UV irradiation (Figure S42). In contrast, macrocycle 1 displays a persistent radical that exhibits a modest amount of radical 26 days after irradiation. In accordance with the spin selection rule, recombination reactions of triplet geminate radical pairs are forbidden and must first undergo ISC to yield a singlet radical pair in order to form products. 27,33 In solution, H-abstraction by BP generally occurs in 10-100 ns, whereas recombination is considered the rate-limiting step (>1 μ s).²⁷ The enhanced stability of these emergent radicals in the solid-state post-UV irradiation is attributed to delocalization of the radical pairs, which is further stabilized by the rigidity of the BP units upon assembly. Studies have shown that self-recombination reactions of the BP ketyl have a rate constant that is an order of magnitude lower than that in cross-reactions.²⁷ This seems to be reflected in the stability of 3 as the ketyl radical signal (g = 2.003) became more prominent the longer the sample remained at room temperature.

Figure 6E,F compares the absorption spectra of triply recrystallized samples (2 and 3) before and after 1 h irradiation. The absorption spectra of both crystalline samples post-UV retained their major spectroscopic properties, although both signals broadened into the visible region. Most intriguingly, irradiation of 2 afforded a new absorbance band at 557 nm, consistent with that in which both the triplet and resulting ketyl absorb. 12,35,36 It should be noted that the triplet state of BP's absorption peak significantly overlaps with its corresponding ketyl; however, the triplet is known to absorb out to wavelengths >600 nm. 35,36 This long wavelength absorption was not observed in the spectra of 3 or 1, 10 again suggesting that UV irradiation of 2 affords increased amounts of radicals versus the other derivatives. Samples of 2 and 3 were analyzed by SC-XRD after UV irradiation and revealed no significant structural changes. Similarly, ¹H NMR spectra were obtained on irradiated samples, showing no spectral changes, which is consistent with the estimated concentration of the radicals (Figures S44 and S45). Finally, the emission behavior of the UV-irradiated crystals was also investigated, with no major changes observed upon excitation at 355 nm (Figure S27).

We have demonstrated that UV irradiation of self-assembled BP-containing molecules can give rise to persistent organic radicals in marked contrast to their behavior in solution. The concentration of the radicals is low but is influenced by structure and assembly, as is their persistence. The parasubstitution of BP-containing radical pairs resulted in longerlived radical species, whereas meta-substituted radical pairs displayed decreased stability. A comprehensive study on a library of BP-containing crystals with varying substituent patterns may be fruitful to further elucidate the rules that govern ketyl radical pair formation and their subsequent stability.

CONCLUSIONS

In summary, three new BP-containing molecules were synthesized, and two afforded single crystals that assembled the photosensitizer through urea-urea hydrogen-bonding interactions. We investigated the impact solid-state assembly has on their photophysics and explored their ability to form persistent radicals as a result of UV irradiation. Solid-state assembly of the materials resulted in a bathochromic shift in both their absorption and emission spectra and quenched their phosphorescent lifetime, which is attributed to BP's selfquenching character. The quantum efficiency of 2 and 3 was <0.3% in solution, although crystallization influenced their quantum yield differently. Crystallization of 2 enhanced its quantum efficiency by an order of magnitude but did not influence 3. TD-DFT calculations on the crystal structures of 2 and 3 in the gas phase and in solution were consistent with these experimental observations. The computations suggested that crystallization of 2 and 3 would influence their photophysical properties differently, predicting a dramatic change in photophysics for 2, and little or no difference was expected for 3.

Self-assembly of compounds 1-3 resulted in three distinct crystal structures that vary the microenvironment around the BP carbonyl. Remarkably, all of the crystalline compounds exhibit persistent radicals upon UV irradiation, even though no radicals were observed in solution. The radical formation is attributed to BP carbonyls' close proximity to neighboring Habstraction sites within the crystal structures. The amount of radicals generated after UV irradiation (1 h) varied 6-fold, with 2 surprisingly showing the largest amount even though only aryl protons with higher BDE are close in proximity (2.60 Å) for abstraction, and macrocycle 1 exhibited the least amount of radicals. Radicals of 2 also displayed the greatest persistence, exhibiting approximately half the EPR signal after 140 days. In

each case, the persistence of the UV-generated radicals was attributed to resonance stabilization about the rigid crystalline framework and may shed light on the impact solid-state assembly has on the recombination of ketyl-containing radical pairs. Future work will be focused on elucidating the factors that govern the formation, stability, and applications of the radicals. We are also exploring the efficiency of these BP sensitizers to undergo triplet-triplet annihilation pathways with molecular oxygen to generate reactive oxygen species.

ASSOCIATED CONTENT

S Supporting Information

The Supporting Information is available free of charge on the ACS Publications website at DOI: 10.1021/jacs.8b08501.

> Synthetic procedures, product characterization, X-ray, photophysical characterization, and EPR spectra (PDF)

X-ray data for triply recrystallized 2 (CIF)

X-ray data for 3 (CIF)

X-ray data for protected 4 (CIF)

X-ray data for protected 2 (CIF)

AUTHOR INFORMATION

Corresponding Author

*shimizls@mailbox.sc.edu

ORCID

Martina De Vetta: 0000-0003-0383-4214 Leticia González: 0000-0001-5112-794X Linda S. Shimizu: 0000-0001-5599-4960

Present Address

§Departamento de Química, Facultad de Ciencias, Universidad Autónoma de Madrid, Madrid, Spain

The authors declare no competing financial interest.

ACKNOWLEDGMENTS

This work was supported in part by the National Science Foundation (CHE-1608874 and OIA-1655740), a Fulbright U.S. Scholar award, and the Marie-Curie Action (TCCM-INT-EJD-642294). We thank Dr. Tom Makris and Dr. Jose Amaya for thrilling EPR discussions.

REFERENCES

- (1) Lehn, J.-M. Proc. Natl. Acad. Sci. U. S. A. 2002, 99, 4763-4768.
- (2) Stupp, S. I.; Palmer, L. C. Chem. Mater. 2014, 26, 507-518.
- (3) Adhikari, B.; Lin, X.; Yamauchi, M.; Ouchi, H.; Aratsu, K.; Yagai, S. Chem. Commun. 2017, 53, 9663-9683.
- (4) Würthner, F.; Kaiser, T. E.; Saha-Möller, C. R. Angew. Chem., Int. Ed. 2011, 50, 3376-3410.
- (5) Würthner, F.; Saha-Möller, C. R.; Fimmel, B.; Ogi, S.; Leowanawat, P.; Schmidt, D. Chem. Rev. 2016, 116, 962-1052.
- (6) Mei, J.; Leung, N. L. C.; Kwok, R. T. K.; Lam, J. W. Y.; Tang, B. Z. Chem. Rev. 2015, 115, 11718-11940.
- (7) Shi, J.; Aguilar Suarez, L. E.; Yoon, S. J.; Varghese, S.; Serpa, C.; Park, S. Y.; Lüer, L.; Roca-Sanjuán, D.; Milián-Medina, B.; Gierschner, J. J. Phys. Chem. C 2017, 121, 23166-23183.
- (8) Lee, S. Y.; Yasuda, T.; Yang, Y. S.; Zhang, Q.; Adachi, C. Angew. Chem., Int. Ed. 2014, 53, 6402-6406.
- (9) Cao, W.; Wang, W. D.; Xu, H.-S.; Sergeyev, I. V.; Struppe, J.; Wang, X.; Mentink-Vigier, F.; Gan, Z.; Xiao, M.-X.; Wang, L.-Y.; Chen, G.-P.; Ding, S.-Y.; Bai, S.; Wang, W. J. Am. Chem. Soc. 2018, 140, 6969-6977.

- (10) DeHaven, B. A.; Tokarski, J. T., III; Korous, A. A.; Mentink-Vigier, F.; Brugh, A. M.; Forbes, M. D. E.; Makris, T. M.; van Tol, J.; Bowers, C. R.; Shimizu, L. S. *Chem. Eur. J.* **2017**, 23, 8315–8319.
- (11) Scott, T. A.; Ooro, B. A.; Collins, D. J.; Shatruk, M.; Yakovenko, A.; Dunbar, K. R.; Zhou, H.-C. Chem. Commun. 2009, 65–67.
- (12) Iwakura, Y.; Takeda, K.; Nakazawa, T.; Watarai, O. J. Polym. Sci., Part B: Polym. Lett. 1968, 6, 115-118.
- (13) Murai, H.; Imamura, T.; Obi, K. Chem. Phys. Lett. 1982, 87, 295–298.
- (14) Fischer, P. H. H.; Zimmermann, H. Z. Naturforsch., A: Phys. Sci. 1968, 23, 1339–1342.
- (15) Dewal, M. B.; Xu, Y.; Yang, J.; Mohammed, F.; Smith, M. D.; Shimizu, L. S. Chem. Commun. 2008, 3909–3911.
- (16) Geer, M. F.; Walla, M. D.; Solntsev, K. M.; Strassert, C. A.; Shimizu, L. S. *J. Org. Chem.* **2013**, *78*, 5568–5578.
- (17) Cai, K.; Xie, J.; Zhang, D.; Shi, W.; Yan, Q.; Zhao, D. J. Am. Chem. Soc. 2018, 140, 5764-5773.
- (18) Mennucci, B. Wiley Interdiscip. Rev.: Comput. Mol. Sci. 2012, 2, 386-404.
- (19) Chai, J. D.; Head-Gordon, M. Phys. Chem. Chem. Phys. 2008, 10, 6615-6620.
- (20) Ditchfield, R.; Hehre, R. W.; Pople, J. A. J. Chem. Phys. 1971, 54, 724–728.
- (21) Simoncelli, S.; Kuzmanich, G.; Gard, M. N.; Garcia-Garibay, M. A. J. Phys. Org. Chem. **2010**, 23, 376–381.
- (22) Kuzmanich, G.; Simoncelli, S.; Gard, M. N.; Spänig, F.; Henderson, B. L.; Guldi, D. M.; Garcia-Garibay, M. A. J. Am. Chem. Soc. 2011, 133, 17296–17306.
- (23) Yuan, W. Z.; Shen, X. Y.; Zhao, H.; Lam, J. W. Y.; Tang, L.; Lu, P.; Wang, C.; Liu, Y.; Wang, Z.; Zheng, Q.; Sun, J. Z.; Ma, Y.; Tang, B. Z. J. Phys. Chem. C 2010, 114, 6090–6099.
- (24) Yang, J.; Zhen, X.; Gao, X.; Ren, Z.; Wang, J.; Xie, Y.; Li, J.; Peng, Q.; Pu, K.; Li, Z. Nat. Commun. 2018, 9, 1–10.
- (25) Gong, Y.; Tan, Y.; Li, H.; Zhang, Y.; Yuan, W.; Zhang, Y.; Sun, J.; Tang, B. Z. Sci. China: Chem. 2013, 56, 1183–1186.
- (26) Marazzi, M.; Mai, S.; Roca-Sanjuán, D.; Delcey, M. G.; Lindh, R.; González, L.; Monari, A. J. Phys. Chem. Lett. 2016, 7, 622–626.
- (27) Dormán, G.; Nakamura, H.; Pulsipher, A.; Prestwich, G. D. Chem. Rev. 2016, 116, 15284–153998.
- (28) Scheffer, J. R. Acc. Chem. Res. 1980, 13, 283-290.
- (29) Ito, Y.; Matsuura, T.; Tabata, K.; Ji-Ben, M.; Fukuyama, K.; Sasaki, M.; Okada, S. *Tetrahedron* **1987**, 43, 1307–1312.
- (30) Hideko, K.; Hessler Bittl, D. P.; Fumihiro, M.; Yang, Y.; Teruo, M. J. Photochem. Photobiol., A 1995, 86, 171–176.
- (31) Buettner, A. V.; Dedinas, J. J. Phys. Chem. 1971, 75, 187-191.
- (32) McMillen, D. F.; Golden, D. M. Annu. Rev. Phys. Chem. 1982, 33, 493-532.
- (33) Woodward, J. R. Prog. React. Kinet. Mech. 2002, 27, 165–207.
- (34) Danielsson, R.; Albertsson, P.-A.; Mamedov, F.; Styring, S. Biochim. Biophys. Acta, Bioenerg. 2004, 1608, 53-61.
- (35) Turro, N. J.; Ramamurthy, V.; Scaiano, J. C. Modern Molecular Photochemistry of Organic Molecules; University Science Books: Sausalito, CA, 2010; pp 483–624.
- (36) Encinas, M. V.; Scaiano, J. C. J. Am. Chem. Soc. 1981, 103, 6393-6397.